

Special Issue “Materiais 2015”

# Shear cohesive law estimation of adhesive layers by digital image correlation

A.C.C. Leitão<sup>a</sup>, R.D.S.G. Campilho<sup>a, \*</sup>, J.C.S. Azevedo<sup>a</sup>

<sup>a</sup>*Departamento de Engenharia Mecânica, Instituto Superior de Engenharia do Porto, Instituto Politécnico do Porto,  
Rua Dr. António Bernardino de Almeida, 431, 4200-072 Porto, Portugal*

## Abstract

Modern and competitive structures are sought to be strong, reliable and lightweight, which increased the industrial and research interest in adhesive bonding. With this joining technique, design can be oriented towards lighter structures. The large-scale application of a given joint technique supposes that reliable tools for design and failure prediction are available. Cohesive Zone Models (CZM) are a powerful tool, although the CZM laws of the adhesive bond in tension and shear are required as input in the models. This work evaluated the value of shear fracture toughness ( $G_{IIC}$ ) and CZM laws of bonded joints. The experimental work consisted on the shear fracture characterization of the bond by a conventional and the  $J$ -integral techniques. Additionally, by the  $J$ -integral technique, the precise shape of the cohesive law is defined. For the  $J$ -integral, a digital image correlation method is used for the evaluation of the adhesive layer shear displacement at the crack tip ( $\delta_s$ ) during the test, coupled to a Matlab<sup>®</sup> sub-routine for extraction of this parameter automatically. As output of this work, fracture data is provided in shear for the selected adhesive, allowing the subsequent strength prediction of bonded joints.

© 2017 Portuguese Society of Materials (SPM). Published by Elsevier España, S.L.U. All rights reserved.

*Keywords:* Adhesive joints; finite element method; cohesive zone models; direct method.

## 1. Introduction

Modern and competitive structures are sought to be strong, reliable and lightweight. With adhesive bonding, design can be oriented towards lighter structures, not only regarding the direct weight saving advantages of the joint over fastened or welded joints, but also because of flexibility to joint different materials. Other advantages include the smaller surface geometry disruption, more uniform stresses along the joint, ease of fabrication, design flexibility and corrosion prevention when bonding different materials [1]. Klarbring [2] showed by an asymptotic analysis that the behaviour of thin adhesive layers between stiff adherends is ruled by elongation,  $w$ , and

shear,  $v$  (whose derivative variables are the normal stress,  $\sigma$ , and shear stress,  $\tau$ , respectively). Many previous studies showed that this simplification is accurate for reproducing the macro-behaviour of adhesive layers. One justification for this, for ductile adhesives in particular, is that the damaged or Fracture Process Zone (FPZ) develops by a significant length beyond the crack tip, which makes the fracture toughness of adhesives not particularly dependent of stresses at the crack tip [3].

The large-scale application of a given joint technique supposes that reliable tools for design and failure prediction are available. Analytical models are limited for damage growth analysis. The concepts of Linear Elastic Fracture Mechanics (LEFM) can be used to analyse fracture of adhesive bonds [4], although involving few limitations: (1) the assumed stress fields are not correctly captured when large-scale plasticity

\* Corresponding author.

*E-mail address:* [raulcampilho@gmail.com](mailto:raulcampilho@gmail.com) (R.D.S.G. Campilho)

is present and (2) in most cases the purpose is to analyse undamaged joints. Thus, these conventional techniques are not the most applicable for bonded joints, unlike CZM, which assume that the FPZ can be described by a law relating the tractions and the physical separations at the crack tip. The cohesive laws are independently characterized for each loading mode and each transition in the global (mixed-mode) law is assessed by different criteria. This technique has been applied to adhesively-bonded structures, in conjunction with development and testing of refined damage onset and failure criteria, different cohesive law shapes and improved cohesive law estimation techniques [5]. The most important step in applying this technique is the estimation of the CZM law, although this is still not standardized [6]. A few data reduction techniques are currently available (the property determination technique, the direct method and the inverse method) that vary in complexity and expected accuracy. In all cases, pure fracture tests, such as the Double-Cantilever Beam (DCB) for mode I and the End-Notched Flexure (ENF), are employed. The property identification method is based on building a parameterized CZM law by isolated materials properties. The main limitation is that the surrounding adherends lead to deviations between the bulk and thin adhesive bond cohesive properties, which are not accounted for [3]. The inverse method relies on a trial and error fitting analysis to experimental data, such as the load-displacement ( $P$ - $\delta$ ) curve of fracture tests, allowing tuning of simplified shape CZM laws for particular conditions [7]. Direct methods output the cohesive law directly from experimental data. Under this scope, the cohesive law is obtained by measuring the  $J$ -integral and crack tip displacements [8] by differentiation of the tensile fracture toughness–tensile displacement ( $G_I$ - $\delta_i$ ) or shear fracture toughness ( $G_{II}$ - $\delta_s$ ) curves. Zhu *et al.* [9] characterized the tensile (DCB) and shear (ENF) cohesive laws of steel/polyurea/steel specimens by the  $J$ -integral/differentiation approach to obtain the rate dependency of these laws considering nominal strain rates between 0.003 and 3 s<sup>-1</sup>. The shear CZM laws were highly nonlinear and strain rate-dependent, which was explained by the interfacial behaviour. This work evaluated the value of  $G_{IIC}$  of bonded joints. The experimental work consisted on the shear fracture characterization of the bond by a conventional and the  $J$ -integral techniques. By the  $J$ -integral technique, the precise shape of the cohesive law is defined. For the  $J$ -integral, a digital image correlation method is used

for the evaluation of  $\delta_s$ , coupled to a Matlab® subroutine for extraction of this parameter automatically.

## 2. Experimental Part

### 2.1. Materials

The aluminium alloy AA6082 T651 was selected for the adherends. The mechanical properties were previously obtained [10]: Young's modulus ( $E$ ) of 70.07±0.83 GPa, tensile yield stress ( $\sigma_y$ ) of 261.67±7.65 MPa, tensile failure strength ( $\sigma_f$ ) of 324±0.16 MPa and tensile failure strain ( $\varepsilon_f$ ) of 21.70±4.24%. The ductile epoxy Araldite® 2015 was selected as the adhesive. A comprehensive mechanical and fracture characterization of this adhesive was recently undertaken [5]. Table 1 presents the relevant mechanical and fracture data of the adhesive.

Table 1. Properties of the adhesive Araldite® 2015 [5].

Property	
Young's modulus, $E$ (GPa)	1.85±0.21
Poisson's ratio, $\nu$	0.33 <sup>a</sup>
Tensile yield strength, $\sigma_y$ (MPa)	12.63±0.61
Tensile failure strength, $\sigma_f$ (MPa)	21.63±1.61
Tensile failure strain, $\varepsilon_f$ (%)	4.77±0.15
Shear modulus, $G$ (GPa)	0.56±0.21
Shear yield strength, $\tau_y$ (MPa)	14.6±1.3
Shear failure strength, $\tau_f$ (MPa)	17.9±1.8
Shear failure strain, $\gamma_f$ (%)	43.9±3.4
Toughness in tension, $G_{IC}$ (N/mm)	0.43±0.02 <sup>b</sup>
Toughness in shear, $G_{IIC}$ (N/mm)	4.70±0.34 <sup>b</sup>

<sup>a</sup> manufacturer's data

<sup>b</sup> estimated in reference [10]

### 2.2. Joint dimensions, fabrication and testing

Fig. 1 shows the geometry and dimensions of the ENF joints: mid-span  $L_H=100$  mm, initial crack length  $a_0 \approx 60$  mm, adherend thickness  $t_p=3$  mm, width  $b=25$  mm and adhesive thickness  $t_A=0.2$  mm.

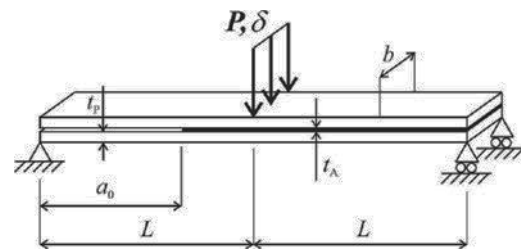


Fig. 1. Geometry of the ENF specimens.

The joints were assembled under controlled conditions of temperature and humidity. The adherends' faces were roughened by grit blasting and cleaned with acetone. Calibrated steel spacers were inserted between the adherends to obtain a constant value of  $t_A$ . Curing was performed at room temperature. The tests were carried out at room temperature in a Shimadzu AG-X 100 testing machine equipped with a 100 kN load cell. For the required test documentation, an 18 MPixel digital camera was used. This procedure made possible obtaining the crack length ( $a$ ) and  $\delta_s$ .

### 3. Data Reduction Schemes for $G_{IIc}$

#### 3.1. Conventional methods

In this work, the following conventional techniques were tested: Compliance Calibration Method (CCM), Direct Beam Theory (DBT), Corrected Beam Theory (CBT) and Compliance-Based Beam Method (CBBM). The CBBM was also considered for the ENF specimen, enabling the estimation of  $G_{IIc}$  only using the experimental compliance, thus not requiring measurement of  $a$ . Details regarding the formulation of these methods are presented in reference [11].

#### 3.2. $J$ -integral method

This section describes the direct method for  $G_{IIc}$  and cohesive law estimation by ENF experiments [9]. This technique relies on the simultaneous measurement of the  $J$ -integral and  $\delta_s$  (Fig. 2). The proposed  $G_{II}$  evaluation expression results from using alternate integration paths to extract the  $J$ -integral:

$$G_{II} = \frac{9 (P_u a)^2}{16 E_a t_p^3} + \frac{3 P_u \delta_s}{8 t_p}, \quad (1)$$

where  $P_u$  is the current load per unit width and  $E_a$  the Young's modulus of the adherends.

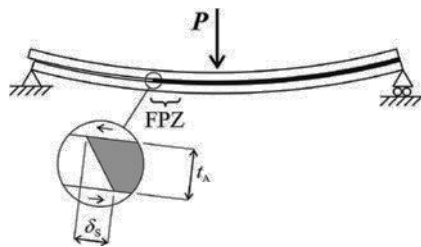


Fig. 2. ENF specimen under loading; detail at the crack tip.

The shear cohesive traction ( $t_s$ )– $\delta_s$  plot or shear cohesive law of the adhesive layer is estimated by

fitting of the  $G_{II}$ – $\delta_s$  law resulting from the application of Eq. (1) and differentiation with respect to  $\delta_s$ .

#### 3.2.1. Measurement of $\delta_s$ by the optical method

A numerical algorithm was developed in a previous work [8], based on digital image processing and tracking reference points by the software to give estimated measurements of  $\delta_s$ . The optical method requires the identification of 6 points: 3 on the top adherend and 3 on the bottom adherend, that enable continuous tracking of the displacements at the crack tip by image capturing at every 5s. For this specific application, the software is programmed to give the value of  $\delta_s$ . The point tracking algorithm is fully automatic, and calculates  $\delta_s$  in pixels, which is then converted to real world units (e.g., mm) by identifying a segment for which the real length is known. More details about this algorithm can be found in reference [8].

## 4. Results

#### 4.1. Conventional methods

The experimental  $P$ – $\delta$  curves revealed a good agreement between specimens (Fig. 3).

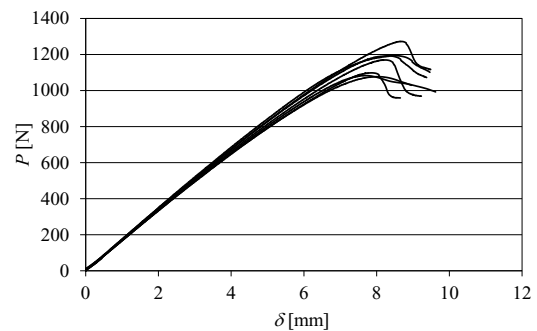


Fig. 3. Experimental ENF test  $P$ – $\delta$  curves.

The CCM requires calculating  $dC/da$  during the test and this is a very critical step, because of the large effect on the outcome of the  $R$ -curve [11]. The  $R$ -curves, which relate  $G_{II}$  vs.  $a$ , are shown in Fig. 4. For all data reduction techniques, the  $R$ -curve is consistent with the theoretically steady-state value of  $G_{II}$  throughout the crack growth phase. The steady-state value of  $G_{II}$  gives a measurement of  $G_{IIc}$ . Another distinctive feature that is patent in Fig. 4 is the deviation to the right of the CBBM curve, which is justified by the inclusion of the FPZ, thus rendering the real crack lengthier than the measured one [11].

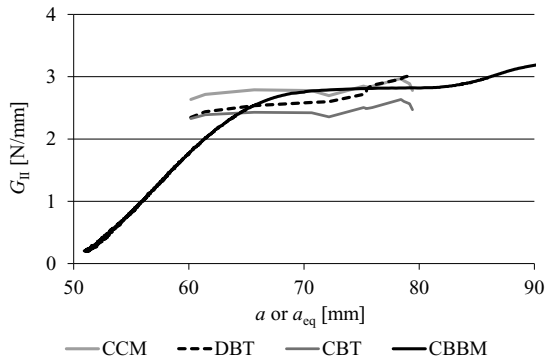


Fig. 4. Representative R-curves for one specimen.

Table 2 summarizes the values of  $G_{IIC}$  (N/mm) of all specimens, considering the average  $G_{II}$  value during the steady-state portion of the curve, and respective average values and deviation for each data reduction technique. Between specimens of the same method, results agree quite well. Additionally, the results between data reduction methods were consistent, except for the CBT (under prediction of 17.0%).

Table 2. Values of  $G_{IIC}$  (N/mm) obtained by all methods.

Adhesive Specimen	Araldite® 2015			
	CCM	DBT	CBT	CBBM
1	3.029	3.083	2.644	3.420
2	-	-	-	-
3	3.675	2.401	2.177	2.545
4	3.214	2.916	2.544	2.943
5	2.812	2.741	2.476	2.801
6	3.357	3.088	2.644	3.136
7	2.696	2.831	2.624	2.901
8	3.008	2.952	2.512	3.025
$\bar{x}$	3.113	2.859	2.517	2.967
$\sigma$	0.334	0.238	0.164	0.273

#### 4.2. J-integral

Initially, the value of  $\delta_s$  was obtained with 5s intervals for each test specimen. Fig. 5 gives a representative example of the variation of  $\delta_s$  with the time elapsed since the beginning of the test. The raw curves from the point tracking algorithm and the adjusted polynomial laws, attained by making  $\delta_s$  (testing time)=0, are included. While the polynomial approximation is necessary to remove the noise from the raw curve, the mentioned procedure to obtain the adjusted polynomial laws was required on account of eventual initial offsets while preparing the specimens that made the  $\delta_s$  value not to be nil at the beginning of each test. It was then possible to estimate the  $G_{II}$ - $\delta_s$  relationship by combining Fig. 5 with the  $G_{II}$  data obtained from Eq. (1).

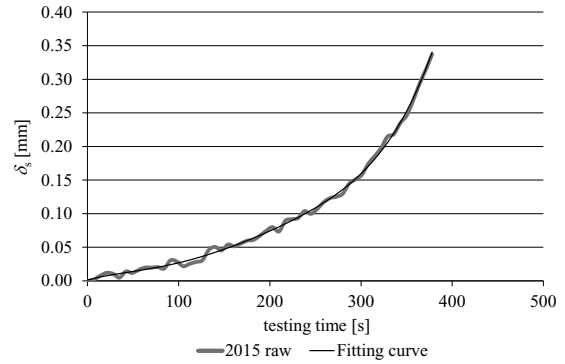


Fig. 5. Plot of  $\delta_s$  – testing time for a specimen.

Fig. 6 shows the  $G_{II}$ - $\delta_s$  curve for the same specimen of Fig. 5 and the selected polynomial approximation.

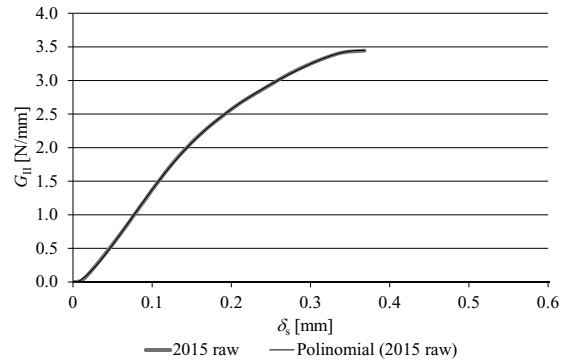


Fig. 6. Plot of  $G_{II}$  –  $\delta_s$  for a specimen.

At the beginning of the test,  $G_{II}$  increases very slowly, but the rate of improvement quickly increases and ultimately a steady-state value is attained. This last stage indicates the onset of crack growth and gives the  $G_{IIC}$  estimate.

Table 3. Values of  $G_{IIC}$  (N/mm) obtained by the J-integral.

Specimen	Araldite® 2015
1	3.444
2	3.585
3	2.873
4	3.298
5	3.123
6	3.140
7	3.080
8	2.901
$\bar{x}$	3.181
$\sigma$	0.249

For the specimen depicted in the figures, the measured value of  $G_{IIC}$  is 3.444 N/mm. The overall results for all specimens are presented in Table 3. The results are consistent with the CBBM of Table 2, with a deviation

between average values of 7.21%. To apply the differentiation procedure, polynomial functions were applied to the raw data of each specimen. Fig. 7 shows the full set of  $t_s$ - $\delta_s$  curves obtained by the direct method.

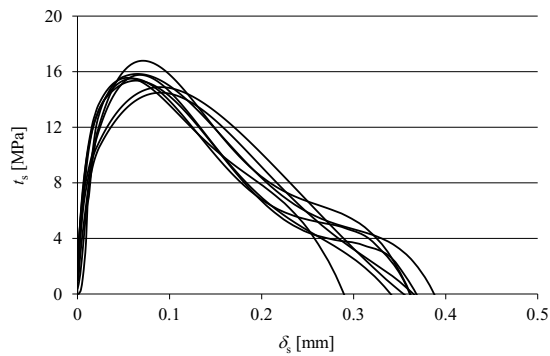


Fig. 7. Comparison of the full set of  $t_s$ - $\delta_s$  curves.

A good agreement was found between curves regarding the initial stiffness of the curves,  $t_s^0$ , descending part of the curves and failure displacement. The average and deviation of the cohesive parameters (with percentile deviation in parenthesis) were as follows:  $t_s^0=15.5\pm 0.683$  MPa (4.4%), displacement at maximum strength  $\delta_s^0=0.0702\pm 0.0122$  mm (17.4%) and displacement at failure  $\delta_{sc}=0.372\pm 0.0246$  mm (6.6%). It can be considered that the scatter between specimens is acceptable. Fig. 8 compares a parametrized trapezoidal CZM law with a representative experimental curve.

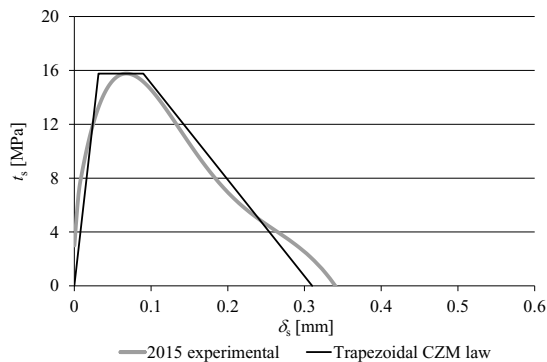


Fig. 8. Comparison of a representative  $t_s$ - $\delta_s$  curve with a simplified trapezoidal CZM law.

## 5. Conclusions

This work addressed the calculation of  $G_{IIC}$  of adhesive joints, considering the ENF test. The tested methods were the CCM, DBT, CBT, CBBM and  $J$ -integral, with the latter enabling the estimation of the shear CZM law of the adhesive. All methods showed a good agreement between specimens. However, between methods, the CBT showed smaller values of  $G_{IIC}$ . Application of the  $J$ -integral, although allowing the estimation of the CZM law by differentiation of the  $G_{II}=f(\delta_s)$  curve, is based on the measurement of  $\delta_s$ , which requires a high-precision technique. However, it has the big advantage of providing complete data for CZM modelling. The shear CZM laws of the adhesive were obtained by the  $J$ -integral. Together with tensile characterization data of this adhesive and mixed-mode damage initiation and propagation criteria, it is possible to predict the strength of bonded joints under generic loading conditions by CZM modelling.

## References

- [1] L.F.M. da Silva, A. Öchsner, R.D. Adams (Ed.), Handbook of Adhesion Technology, Springer, Heidelberg, 2011.
- [2] A. Klarbring, Int. J. Eng. Sci. 29 (1991) 493.
- [3] T. Andersson, U. Stigh, Int. J. Solids Struct. 41 (2004) 413.
- [4] E. Ripling, S. Mostovoy, R. Patrick, ASTM STP-360, (1964) p. 5.
- [5] R.D.S.G. Campilho, M.D. Banea, J.A.B.P. Neto, L.F.M. da Silva, J. Adhes. 88 (2012) 513.
- [6] M.J. Lee, T.M. Cho, W.S. Kim, B.C. Lee, J.J. Lee, Int. J. Adhes. Adhes. 30 (2010) 322.
- [7] R.D.S.G. Campilho, M.F.S.F. de Moura, A.M.G. Pinto, J.J.L. Morais, J.J.M.S. Domingues, Composites, Part B: Engineering 40 (2009) 149.
- [8] R.D.S.G. Campilho, D.C. Moura, D.J.S. Gonçalves, J.F.M.G. da Silva, M.D. Banea, L.F.M. da Silva, Composites, Part B: Engineering 50 (2013) 120.
- [9] Y. Zhu, K.M. Liechti, K. Ravi-Chandar, Int. J. Solids Struct. 46 (2009) 31.
- [10] R.D.S.G. Campilho, M.D. Banea, A.M.G. Pinto, L.F.M. da Silva, A.M.P. de Jesus, Int. J. Adhes. Adhes. 31 (2011) 363.
- [11] M.F.S.F. de Moura, R.D.S.G. Campilho, J.P.M. Gonçalves, Int. J. Solids Struct. 46 (2009) 1589.